RSC Chemical Biology

ROYAL SOCIETY OF CHEMISTRY

PAPER

View Article Online
View Journal | View Issue

Cite this: *RSC Chem. Biol.*, 2023, **4**, 414

Radiolabeling and *in vivo* evaluation of lanmodulin with biomedically relevant lanthanide isotopes†

Kirsten E. Martin,[a] Joseph A. Mattocks,[b] Dariusz Śmiłowicz,[a] Eduardo Aluicio-Sarduy,[cd] Jennifer N. Whetter,[a] Jonathan W. Engle,[cd] Joseph A. Cotruvo Jr *[b] and Eszter Boros *[a]

Short-lived, radioactive lanthanides comprise an emerging class of radioisotopes attractive for biomedical imaging and therapy applications. To deliver such isotopes to target tissues, they must be appended to entities that target antigens overexpressed on the target cell's surface. However, the thermally sensitive nature of biomolecule-derived targeting vectors requires the incorporation of these isotopes without the use of denaturing temperatures or extreme pH conditions; chelating systems that can capture large radioisotopes under mild conditions are therefore highly desirable. Herein, we demonstrate the successful radiolabeling of the lanthanide-binding protein, lanmodulin (LanM), with medicinally relevant radioisotopes: ^{177}Lu, $^{132/135}$La and ^{89}Zr. Radiolabeling of the endogenous metal-binding sites of LanM, as well exogenous labeling of a protein-appended chelator, was successfully conducted at 25 °C and pH 7 with radiochemical yields ranging from 20–82%. The corresponding radiolabeled constructs possess good formulation stability in pH 7 MOPS buffer over 24 hours (>98%) in the presence of 2 equivalents of ^{nat}La carrier. *In vivo* experiments with [^{177}Lu]-LanM, [$^{132/135}$La]-LanM, and a prostate cancer targeting-vector linked conjugate, [$^{132/135}$La]-LanM-PSMA, reveal that endogenously labeled constructs produce bone uptake *in vivo*. Exogenous, chelator-tag mediated radiolabeling to produce [^{89}Zr]-DFO-LanM enables further study of the protein's *in vivo* behavior, demonstrating low bone and liver uptake, and renal clearance of the protein itself. While these results indicate that additional stabilization of LanM is required, this study establishes precedence for the radiochemical labeling of LanM with medically relevant lanthanide radioisotopes.

Received 14th February 2023,
Accepted 4th April 2023

DOI: 10.1039/d3cb00020f

rsc.li/rsc-chembio

Introduction

Emerging radioactive lanthanide isotopes such as ^{177}Lu (β^-(max) = 501 keV, $t_{1/2}$ = 6.64 d), ^{86}Y (β^+(max) = 4.2 MeV, $t_{1/2}$ = 14.7 h), ^{161}Tb (β^-(max) = 593 keV, $t_{1/2}$ = 6.90 d) and ^{132}La ($t_{1/2}$ = 4.59 h, 42.1% β^+(max) = 3.67 MeV) offer promising avenues for the development of diagnostic and therapeutic radiopharmaceuticals.[1] In order to selectively deliver these radionuclides to a target organ or tissue, they must be appended to a tissue/organ-specific targeting vector by way of a bifunctional chelator.[2,3] Such chelators, once bound to the metal ion of interest, must exhibit high kinetic inertness to prevent isotope release prior to delivery. In many instances, and for most clinically used radiopharmaceuticals, this is achieved by use of macrocycle- or cryptand-based chelator systems that rigidify upon binding of the metal ion, forming exceptionally inert coordination complexes.[4–7] However, the high thermodynamic stability of the corresponding chelate, combined with conformational changes required to form an in-cage chelate complex, often necessitates incubation at 80–100 °C for prolonged periods of time (1–2 hours).[8–11] This poses no issue when the targeting vector is a small molecule or short peptide with good thermal stability. However, if biological targeting vectors such as monoclonal antibodies, antibody fragments, or affibodies are employed, the requirement for heating poses a significant challenge. This must be addressed by combining such targeting vectors with bifunctional chelators that form inert complexes at <40 °C with high radiochemical yield and

[a] *Department of Chemistry, Stony Brook University, Stony Brook, New York 11794, USA. E-mail: eszter.boros@stonybrook.edu*
[b] *Department of Chemistry, The Pennsylvania State University, University Park, Pennsylvania 16802, USA. E-mail: juc96@psu.edu*
[c] *Department of Medical Physics, University of Wisconsin, Madison, Wisconsin 53705, USA*
[d] *Department of Radiology, University of Wisconsin, Madison, Wisconsin 53705, USA*

† Electronic supplementary information (ESI) available. See DOI: https://doi.org/10.1039/d3cb00020f

purity – a challenge which remains pertinent, especially for lanthanide isotopes.[12–14]

To date, few chelators have been employed to chelate large lanthanides under mild conditions, outlining a need for the development of such systems.[15] Our group has previously investigated the chelation and targeted delivery of the ^{132}La/^{135}La pair.[16] The ^{132}La isotope is suitable for positron emission tomography (PET), while ^{135}La ($t_{1/2}$ = 18.9 h) decays by electron capture with the subsequent emission of 10.9 ± 3.2 high linear energy transfer (LET) Auger electrons per decay.[17] These electrons travel less than a micron in tissue on average, suitable for targeted radiotherapy.[18] Furthermore, due to the comparable size and chemical behavior to the Ac^{3+} ion, the La^{3+} ion and its isotopes are considered suitable surrogates to facilitate the development of ^{225}Ac radiopharmaceuticals in light of the ^{225}Ac isotope's scarcity and lack of imageable emissions.[16,19] The ^{135}La and ^{132}La isotopes are produced concomitantly when ^{nat}Ba is irradiated with protons. Our previous work found that functionalized, tetra-azamacrocycle derived chelators required prolonged incubation at 80 °C to produce in cage formation, while the large cavity macrocycle macropa enabled room-temperature chelation but suffered from radiolytic degradation of the chelate-adjacent, peptide-linked thiourea bond in its functionalized state.[16] Thus, alternative approaches, especially to $^{132/135}$La chelation of bioconjugates, remain elusive.

Lanmodulin (LanM) is a 12 kDa protein, produced by methylotrophic bacteria that preferentially acquires and utilizes the lighter, larger lanthanides for essential functions. LanM possesses three highly selective lanthanide-binding sites with average apparent dissociation constants (K_d) in the low picomolar range across the lanthanide series (at pH 7.2, ranging from 1.8 pM for La^{3+} to ~5-fold higher for Ho^{3+} (the heaviest lanthanide for which the apparent K_d has been directly measured; the apparent K_d for Lu^{3+} is expected to be slightly weaker)).[20–22] These apparent K_d values represent the two tightest, cooperative metal-binding sites (EF-hands 2 and 3); EF-hand 1 is ~4-fold weaker in the case of La^{3+},[20,23] and it is more susceptible to disruption by competing ligands.[23–25] The protein itself is stable under extreme pH and thermally challenging conditions.[20,26] LanM exhibits a large, cooperative, and highly selective conformational response to lanthanides that results in a shift from a disordered secondary structure to ~60% alpha-helical character, a structure that retains the metal ions in their respective binding pockets with appropriate kinetic inertness.[27] These properties have been leveraged for applications ranging from the sequestration and separation of rare earths from electronic waste[24,26] to separation of trivalent actinides and lanthanides from di- or tetravalent contaminants on the macroscopic scale.[28,29] Long-term cycling of LanM for the purification of ^{228}Ac further demonstrated LanM's considerable resilience against radiolytic degradation.[22] Additionally, through modification of metal-binding site, LanM can be tuned to possess enhanced selectivity for actinides over lanthanides (Cm *vs.* Eu).[25]

Based on the exceptional selectivity and resilience of LanM complexes with large lanthanides like La^{3+} against physiological competing chelators such as phosphate,[20,22,26] achieved at biocompatible temperatures <40 °C, paired with stabilization of the metal-bound LanM species within a broad pH range, we hypothesized that the LanM protein could provide a suitable alternative to small molecular chelates with radiosensitive bifunctionalization handles for the radiolabeling and targeted delivery of biomedically relevant lanthanide isotopes. Herein, we demonstrate the endogenous and exogenous radiolabeling of LanM with ^{177}Lu (endogenous), $^{132/135}$La (endogenous), and ^{89}Zr (exogenous), as well as the synthesis of [$^{132/135}$La]-LanM-PSMA, a LanM protein functionalized with a prostate cancer targeting peptide (Fig. 1). The corresponding radiolabeled constructs were probed for their *in vitro*, *in vivo*, and metabolic stabilities to determine the potential of LanM for the chelation and targeted delivery of the biomedical isotope $^{132/135}$La at tracer scale.

Experimental

Materials and methods

All chemicals were obtained from commercial suppliers in biochemical reagent grade or better and used without further

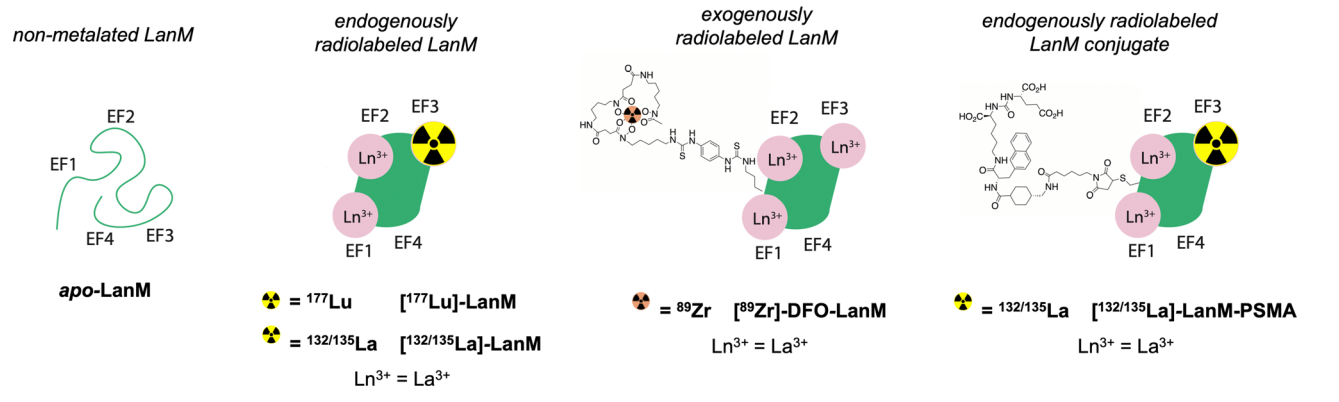

Fig. 1 Schematic description of LanM variants subject of this work, including unfolded, non-metalated LanM, endogenously radiolabeled, folded LanM, exogenously radiolabeled, folded LanM and endogenously labelled LanM conjugated to a targeting peptide *via* modified, N-terminal cysteine-maleimide. Note: we are unable to localize incorporation of isotope to a specific site of EF1, EF2, and EF3 in the endogenously labeled LanM; schematic descriptions only include EF3 labelled for simplicity, in this and in subsequent figures.

purification. *E. coli* BL21(DE3) cells were obtained from New England Biolabs (NEB). NMR spectra (^{1}H, ^{13}C) were collected on a 700 MHz Advance III Bruker instrument at 25 °C and processed using TopSpin 4.0.7. Chemical shifts are reported as parts per million (ppm). Mass spectrometry of protein constructs was performed at the Proteomics and Mass Spectrometry Core Facility at Pennsylvania State University. The mass spectra were acquired on a Bruker Ultraflextreme MALDI TOF–TOF instrument using a factory-configured instrument method for the linear positive-ion detection over the 5000–20 000 m/z range. Laser power attenuation and pulsed ion extraction time were optimized to achieve the best signal. The instrument was calibrated with a five-protein mixture containing bovine insulin (M_W 5733.6), bovine ubiquitin (M_W 8564.8), horse heart cytochrome *C* (M_W 12 360.1), bovine ribonuclease A (M_W 13 682.3), and horse heart apomyoglobin (M_W 16 951.5). Mass spectra were smoothed (Savitzky–Golay, width 5 m/z, 1 cycle) and baseline subtracted (TopHat). Mass lists were generated using a centroid peak detection algorithm. High-resolution electrospray ionization (ESI) mass spectrometry of small molecules was carried out at the Stony Brook University Center for Advanced Study of Drug Action (CASDA) with a Bruker Impact II UHR QTOF MS system. Gel filtration chromatography was performed on an automated GE Healthcare Biosciences Akta Pure fast protein liquid chromatography system (FPLC). Preparative high performance liquid chromatography (HPLC) was carried out on a Phenomenex Luna C18 column (250 mm × 21.2 mm, 100 Å, AXIA packed) at a flow rate of 15 mL min^{-1} using a Shimadzu HPLC-20AR equipped with a binary gradient pump, UV-vis detector, and manual injector. UV absorption was recorded at 254 nm. Method A (Solvent A = H_2O + 0.1% TFA and B = MeCN + 0.1% TFA): Gradient: 0–1 min: 5% B; 1–14 min: 5–50% B; 14–23 min: 50–95% B; 23–26 min: 95% B; 26–27 min: 95–5% B; 27–30 min: 5% B. Analytical HPLC was carried out on a Phenomenex Luna 5 μm C18 column (150 mm × 3 mm, 100 Å, AXIA packed) at a flow rate of 0.8 mL min^{-1} using a Shimadzu HPLC-20AR equipped with a binary gradient pump, UV-vis detector, autoinjector, and Laura radiodetector. Method B (Solvent A = H_2O + 0.1% TFA and B = MeCN + 0.1% TFA): Gradient: 0–2 min: 5% B; 2–14 min: 5–95% B; 14–16 min: 95% B; 16–16.5 min: 95–5% B; 16.5–20 min 5% B. RadioHPLC analysis was carried out on the Shimadzu HPLC-20AR equipped with a binary gradient, pump, UV-Vis detector, autoinjector and a Laura radiodetector on a Phenomenex Yarra-2000 size exclusion column using an isocratic gradient (Method C: 3 μm, 145 Å, 150 × 7.8 mm; Solvent: 30 mM MOPS (3-(*N*-morpholino)-propanesulfonic acid), 100 mM KCl, pH = 7.0; 0.75 mL min^{-1}). Inductively coupled plasma optical emission spectroscopy (ICP-OES) was carried out using an Agilent 5110 inductively coupled plasma optical emission spectrometer. A 6-point standard curve with a check standard with respect to lutetium and lanthanum was used and fits were found to be at least R^2 of 0.9999. Concentrations were then back calculated to the sample stock concentration. PET imaging was conducted using Siemens Inveon PET/CT Multimodality System and data reconstruction was done using ASIPro software and AMIDE. $^{177}LuCl_3$ was obtained from the Department of Energy (DOE) isotope program, produced at the University of Missouri reactor. $^{132/135}LaCl_3$ and ^{89}Zr-oxalate were obtained from the Engle Lab at University of Wisconsin–Madison.

Expression and purification of LanM variants

Wild type (WT) LanM was produced as described.[30] Cys-LanM (WT-LanM with a Gly-Ser-Gly-Cys peptide added to the C-terminus) was purified as described.[31] Briefly, plasmids containing genes encoding for each protein were obtained from TWIST Bioscience (pET-29b(+)-LanM). The proteins were grown in chemically competent *E. coli* BL21(DE3) cells (NEB), which were grown at 37 °C in Lysogeny broth (LB). Isopropyl β-D-1-thiogalactopyranoside (IPTG, 200 μM) was added at $OD_{600\,nm}$ = ~0.6 to induce overexpression for 3 h at 37 °C. Cells were lysed by sonication and loaded to a gravity-flow 25 mL (2.5 × 5 cm) Q-Sepharose Fast Flow column and eluted using an 80 × 80 mL, 0.01–1 M NaCl gradient. Dithiothreitol (DTT, 10 mM) was included in these buffers for Cys-LanM purification to minimize thiol oxidation. LanM-containing fractions were identified by SDS-PAGE analysis and then purified using gel filtration chromatography (HiLoad 16/600 Superdex 75 pg). For Cys-LanM purifications, 5 mM DTT was included. LanM- or Cys-LanM-containing fractions were collected and concentrated to ~2.0 mM. LanM was stored in 30 mM MOPS, 100 mM KCl, 5% glycerol, pH 7.0 and Cys-LanM was stored in the same buffer containing 5 mM DTT.

Chemical functionalization of LanM and Cys-LanM

LanM-PSMA. PSMA-mal was dissolved in pure dimethyl sulfoxide (DMSO, ~25 mg mL^{-1} or 25 mM). In a 1.7 mL tube, 222 μL Cys-LanM (1.8 mM) and 650 μL buffer (50 mM Tris, 100 mM KCl, 10 mM tris(2-carboxyethyl)phosphine, TCEP, pH 7.4) were mixed and incubated for 2 min. Then, 128 μL of PSMA-mal (25 mM, 8 eq. relative to LanM, for preparation and characterization see ESI†) were added dropwise over 1 min while mixing to prevent precipitation. The reaction mixture was nutated at 4 °C overnight. The resulting mixture was centrifuged at 12 000 ×*g* for 2 min to remove precipitate. The reaction product was confirmed in the remaining aqueous phase by mass spectrometry and subsequently purified using analytical-scale gel filtration chromatography (HiLoad 10/300 Superdex 75 pg, 1 mL loop, 0.75 mL min^{-1}) using 30 mM MOPS, 100 mM KCl, 5% glycerol, pH 7.0 (no reductant). The protein conjugate eluted from the column over the course of 2 mL.

DFO-LanM. p-SCN-Bn-desferrioxamine (DFO-NCS) (752.9 g mol^{-1}) was obtained from Macrocyclics, Inc. and dissolved in pure DMSO (~20 mg mL^{-1} or 25 mM). In a 15 mL conical tube, 5.4 mL of 100 mM KCl, 500 μL LanM (2.0 mM stock concentration), and 8.0 μL $LaCl_3$ (250 mM stock concentration) were combined to produce La_2LanM. To this mixture, 4.0 mL of 100 mM $NaHCO_3$, 100 mM KCl, pH 9.0 was added. This order of addition is important to prevent precipitation of lanthanum carbonate. Finally, 10 × 10 μL additions of DFO-NCS (25 mM or 5 mg per 264 μL) were added, with thorough mixing between each addition. Final reaction mixture was 100 μM La_2LanM and

250 μM DFO-NCS (2.5 eq. of DFO-NCS relative to La_2LanM), which was nutated overnight at room temperature. Product was spun down (12 000 ×*g* for 2 min) to remove precipitate and concentrated to ~400 μL using an Amicon Ultra 10 kDa molecular weight cup off (MWCO) centrifugal filter device. >50% incorporation of DFO-NCS was confirmed by mass spectrometry through formation of peaks at *m*/*z* values integer multiples of 752 above LanM base mass of 11 686 Da (Fig. S5, ESI†).

Radiochemical labeling

Lu-177 labeling. Radiolabeling with ^{177}Lu was performed by mixing 37 MBq (1.0 mCi ^{177}Lu for ^{177}Lu–Lu-LanM) or 126 MBq (3.40 mCi ^{177}Lu for ^{177}Lu–La-LanM) with 20 nmol of apo-protein in 30 mM MOPS, 100 mM KCl, pH 7.0. Subsequently, 2 equivalents of non-radioactive metal ($LuCl_3$, 8 μL, 5.0 mM or $LaCl_3$, 10.3 μL, 3.88 mM) were added. Samples were allowed to react for 90 min at room temperature and then purified using Zeba spin desalting columns (7k MWCO). A radiochemical yield of 75.4% for ^{177}Lu–Lu-LanM and 20.6% for ^{177}Lu–La-LanM were achieved.

La-132/135 labeling. Radiolabeling with $^{132/135}$La was performed by mixing 11 MBq (0.3 mCi $^{132/135}$La) of radiometal with 20 nmol of apo-protein in 30 mM MOPS, 100 mM KCl, 5% glycerol, pH 7.0. Subsequently, 2 equivalents of non-radioactive metal ($LaCl_3$, 7.6 μL, 5.22 mM) were added. Samples were allowed to react for 90 min at room temperature and then purified using Zeba spin desalting columns (7k MWCO). A radiochemical yield of 28.4% was achieved.

Zr-89 labeling. ^{89}Zr-oxalate was pH-adjusted using 0.1 M Na_2CO_3 to pH 7.0. Radiolabeling with ^{89}Zr was then performed by mixing 35.7 MBq (965 μCi ^{89}Zr) of radiometal with 20 nmol of La_2LanM in 30 mM MOPS, 100 mM KCl, pH 7.0. Samples were allowed to react for 90 min at room temperature and then purified using Zeba spin desalting columns (7k MWCO). A radiochemical yield of 82.5% yield was achieved.

***In vivo* experiments and metabolite analysis.** All animal experiments were approved by and conducted according to the guidelines of the Institutional Animal Care and Use Committee (IACUC) at Stony Brook Medicine.

General procedure for naïve biodistribution and metabolite analysis. Male mice (6 weeks old, Charles River, BALB/C) were injected with radiolabeled LanM (0.9–1.5 MBq/25–40 μCi), or unbound radiometal (1.2–1.6 MBq/32–43 μCi). After 2 h, animals were sacrificed by cervical dislocation and selected tissues were collected and weighed. Activity of tissues was counted using a γ-counter (1470 PerkinElmer Wizard) and the radioactivity associated with each organ was expressed as % ID/g. To assess the presence of intact protein remaining, urine was directly injected to the radioHPLC and the resulting trace was compared to that of the radiolabeled protein.

General procedure for biodistribution and metabolite analysis in murine xenograft model. Male mice (5 weeks old, Taconic, NCr nude male) were inoculated subcutaneously with PSMA+ PC-3 PiP cells and PSMA− PC-3 flu cells (5.0×10^5 each) suspended in Matrigel and DPBS (1 : 2 DPBS: Matrigel), on the right and left shoulders respectively. When tumors reached a suitable size (<200 mm^3), mice were injected with the radiolabeled species of interest and biodistribution/metabolite analysis was conducted in accordance with biodistribution studies in naïve mice.

Results and discussion

Synthesis of LanM-PSMA and DFO-LanM conjugates

To enable targeting or exogenous labeling of LanM, we conducted chemical functionalization of LanM *via* the native N-terminus (and lysine sidechains) and Cys-LanM, a mutant incorporating a surface accessible cysteine at the C-terminus for facile bioconjugation.[24] Previous work showed that the C-terminally Cys-modified LanM exhibits similar metal-binding properties to the wild-type protein.[24]

To functionalize LanM with a disease-specific targeting vector, the protein was conjugated to a short, peptide-based targeting vector selective for the prostate specific membrane antigen (PSMA), a well-studied antigen overexpressed on the surface of prostate cancer cells.[32–35] In addition to the well-established nature of the corresponding targeting vector's chemistry, a wealth of *in vivo* imaging and biodistribution data has been reported on PSMA-targeted constructs; therefore, previously published datasets serve as suitable means to evaluate the relative stability and performance of new PSMA-targeting entities. A maleimide-functionalized version of the small peptide targeting vector used in the clinically approved ^{177}Lu-PSMA-617 was synthesized with manual solid phase peptide synthesis methods (Fig. S3, ESI†).[36] With established maleimide–thiol coupling conditions, this maleimide linked-PSMA targeting vector was subsequently appended to Cys-LanM, to produce LanM-PSMA. Successful conjugation was affirmed by mass spectrometric analysis (Fig. S4, ESI†).

In addition to LanM-PSMA, we also proposed the synthesis of a LanM conjugate to selectively incorporate a radionuclide *via* exogenous radiolabeling of fully metalated LanM. An exogenously tagged construct can provide information on the protein's native pharmacokinetic behavior without concern of potential metal dissociation from the endogenous metal-binding sites. To this end, we employed desferrioxamine (DFO), a chelator with poor affinity for large, trivalent lanthanides but high affinity for the Zr^{4+} ion.[37] Antibody-linked DFO is commonly employed for the chelation of the ^{89}Zr PET isotope (β^+(max) = 897 keV, $t_{1/2}$ = 78 hours).[38] In a similar manner to well-established antibody conjugation, DFO-NCS was appended to LanM *via* available and reactive lysine side chains (and/or the N-terminus) and formed the corresponding thiourea bond (Fig. S5, ESI†).[39] Formation of the desired conjugate was confirmed using mass spectrometric analysis, revealing the formation of multiple LanM-DFO conjugates (LanM(DFO)$_n$, n = 1–3).

Endogenous radiochemical labeling of Ln binding sites

To investigate the feasibility of radiolabeling LanM within its metal-binding sites, we probed radiochemical labeling with the largest and smallest lanthanides, La^{3+} and Lu^{3+}, both of which

possess readily available radioisotopes, $^{132/135}$La and ^{177}Lu, respectively.

Radiolabeling of LanM (10 nmol) was achieved with ^{177}Lu at room temperature in 90 minutes using a low-specific-activity radiolabeling approach by addition of ^{nat}Lu. Initial attempts to radiolabel LanM at tracer concentration (<5 pmol) led to no significant incorporation of the isotope. We posited that at tracer levels, the binding of (statistically) no more than one metal ion per LanM protein did not allow for a cooperative conformational change, which has been documented to stabilize the metal–protein complex.[20,23] Therefore, we proceeded with a cold-carrier-mediated radiolabeling approach.

To probe the optimal quantity of non-radioactive metal necessary to maximize radiolabeling yields, apo-LanM was incubated with 1–4 equivalents of ^{nat}Lu (cold carrier) relative to protein quantity in presence of ^{177}Lu (0.1 mCi). Two equivalents of carrier ^{nat}Lu produced the most labeled protein (Fig. S7, ESI†) according to radioHPLC size exclusion chromatography (SEC) analysis (Fig. 2A). After radiolabeling, unbound metal was separated from [^{177}Lu]-LanM using size exclusion chromatography to produce the purified, endogenously labeled construct in 75% isolated radiochemical yield (RCY). We also assessed the achievable radiochemical yield using ^{nat}La as the non-radioactive carrier, which also resulted in formation of the desired product, albeit with only 20% radiochemical labeling yield, possibly due to preferential incorporation of the larger La^{3+} ion over trace $^{177}Lu^{3+}$. Formulation stability measurements over 24 hours indicated that ^{nat}La carrier resulted in good retention of radioactivity within the protein, whereas ^{nat}Lu resulted in release of the radioactive metal ion over the same time course (Fig. 2B and C). This result may be explained by Lu^{3+} being the lanthanide that is least efficient in inducing LanM's conformational change, and/or that formation of Lu hydroxides occurs over long periods of time because of the presence of two solvent molecules in the metal-binding sites.[28]

Accordingly, radiolabeling of apo-LanM with $^{132/135}$La was conducted using 2 equivalents of ^{nat}La carrier and the crude reaction mixture was purified using size exclusion chromatography. The purified [$^{132/135}$La]-LanM was obtained in 28% radiochemical yield. Both [^{177}Lu]-LanM and [$^{132/135}$La]-LanM with ^{nat}La as non-radioactive carrier exhibited excellent formulation stability in pH 7.4 MOPS buffer (compatible with *in vivo* injection) for 24 hours.

Exogenous radiochemical labeling

The exogenous radiochemical labeling of DFO-LanM (for synthesis and characterization *vide supra*) was conducted using DFO-LanM with fully occupied LanM metal binding sites using 3 equivalents of ^{nat}La. Radiolabeling with ^{89}Zr was carried out without the addition of additional non-radioactive carrier to form [^{89}Zr]-DFO-LanM at room temperature and pH 7, followed by separation and isolation of the product with an 83% radiochemical labeling yield using size exclusion chromatography (Fig. 3).

In vivo biodistribution in naïve mice

One of the most important evaluation criteria of new radiochemical labeling methods involves the determination of *in vivo* pharmacokinetics and stability of the corresponding labeled constructs. To this end, we administered the radiolabeled [$^{132/135}$La]-LanM, [^{177}Lu]-LanM and ^{89}Zr-DFO-LanM intravenously to naïve, balb/C mice, followed by biodistribution and urine metabolite analysis 2 hours post injection. Additional cohorts received [^{177}Lu]$LuCl_3$, [$^{132/135}$La]La-citrate or ^{89}Zr-oxalate to determine the corresponding metal ion's native biodistribution. As expected and in accordance with previous studies, the administration of [^{177}Lu]$LuCl_3$ results in significant bone (8.30 ± 4.47% ID/g, Fig. 4A) and liver uptake (19.27 ± 0.69% ID/g, Fig. 4A). ^{177}Lu-LanM demonstrates similar bone uptake (8.89 ± 3.15% ID g^{-1}), indicative of likely dissociation of ^{177}Lu from the metal binding sites within LanM during *in vivo* circulation. In contrast, *in vivo* administration of [$^{132/135}$La]-LanM results in enhanced renal clearance and significant reduction of bone uptake (3.53 ± 0.49% ID g^{-1}) when compared to results obtained with the free ion control [$^{132/135}$La]La-citrate (9.07 ± 1.89% ID g^{-1}). These results indicate a better retention of La^{3+}, over the smaller Lu^{3+} (1.21 *vs.* 0.98 Å, CN = 8) in accordance with the protein's native selectivity and higher binding affinity for the former (Fig. 4B) and are also consistent with the greater stability of LanM complexes with larger Ln^{3+} ions against competitors, such as citrate, which is present in serum. Urine metabolite analysis using SEC-HPLC detected intact, radiometalated protein for both studies (Fig. 4D and E).

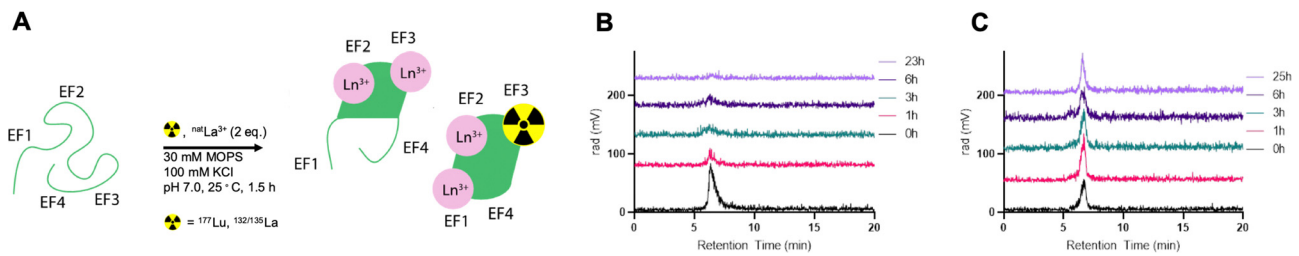

Fig. 2 (A) Schematic description of carrier-added radiochemical labeling procedure for the introduction of ^{177}Lu or $^{132/135}$La to the endogenous metal ion binding sites of LanM. (B) Formulation stability analysis using SEC-radioHPLC of [^{177}Lu]-LanM using ^{nat}Lu as non-radioactive carrier shows the degradation of the LanM-associated peak over the course of the experiment while (C) shows retention of the ^{177}Lu isotope within the endogenous LanM metal ion binding site with ^{nat}La as the non-radioactive carrier.

Fig. 3 Schematic description of no carrier-added radiochemical labeling procedure for the introduction of 89Zr to the exogenous, DFO metal ion binding site of DFO-LanM.

To further assess the protein's native distribution *in vivo*, we conducted the biodistribution analysis of [^{89}Zr]-DFO-LanM. [^{89}Zr]-DFO-LanM resulted in low bone uptake (0.48 ± 0.07% ID/g) compared to the $^{89}Zr^{4+}$-oxalate (6.23 ± 4.35% ID/g) and primarily kidney uptake, indicating renal clearance of [^{89}Zr]-DFO-LanM (Fig. 4C). This behavior is comparable to that observed for similarly sized ^{89}Zr-labeled Fab fragments or single-chain variable fragments (scFv's). [^{89}Zr]-DFO-LanM did not result in significant accumulation in liver and bone tissues, indicating that *in vivo* dissociation of a fraction of $^{132/135}$La and, especially, ^{177}Lu from endogenous labeling sites within LanM is likely. Urine metabolite analysis using SEC-HPLC also detected intact, radiometalated protein (Fig. 4F) for the [^{89}Zr]-DFO-LanM species.

Imaging and biodistribution of LanM-PSMA in a mouse xenograft model

Radiolabeling of LanM-PSMA with $^{132/135}$La was conducted in accordance with the previously established, $^{nat}La^{3+}$ carrier-added method to afford [$^{132/135}$La]-LanM-PSMA. We carried out cell binding experiments, to probe if [$^{132/135}$La]-LanM-PSMA could retain binding to its target. PC3 PiP (PSMA+ cells) and PC3 Flu (PSMA− cells) were incubated with [$^{132/135}$La]-LanM-PSMA for two hours.[40,41] While significantly higher uptake was observed in PSMA+ cells when compared to PSMA− cells (1.97% and 1.00%, respectively, $p < 0.0001$, Fig. 5), overall uptake was reduced compared to the binding affinity observed for [^{68}Ga]-PSMA-617 (~16%).[42] The source of this reduced affinity is possibly two-fold: decreased affinity to the target due to interference of the LanM protein with efficient binding to the cell surface antigen and/or the slow dissociation of the $^{132/135}$La isotope from the endogenous metal ion binding site over the course of the cell binding experiment.

As [$^{132/135}$La]-LanM-PSMA showed enhanced uptake in PSMA-expressing cells, we proceeded to *in vivo* assessment in a bilateral xenograft model. [$^{132/135}$La]-LanM-PSMA was administered to NCr athymic nude mice bearing PC3 PiP (PSMA+ cells) and PC3 Flu (PSMA− cells) xenografts on the left and right shoulders, respectively. Biodistribution analysis conducted at the 2 hour post injection time point shows localization of the activity in kidneys and bladder (Fig. S15, ESI†). [$^{132/135}$La]-LanM-PSMA resulted in 97.74 ± 50.10% ID/g in the kidneys, in comparison with 9.86 ± 3.89% ID/g in the [$^{132/135}$La]-citrate cohort, mirroring the protein's native renal clearance and indicating that some fraction of $^{132/135}$La is likely retained within the protein. However, this study further affirmed that *in vivo* circulation also resulted in release of $^{132/135}$La from the endogenous binding site, as significant high bone uptake for [$^{132/135}$La]-LanM-PSMA, comparable to

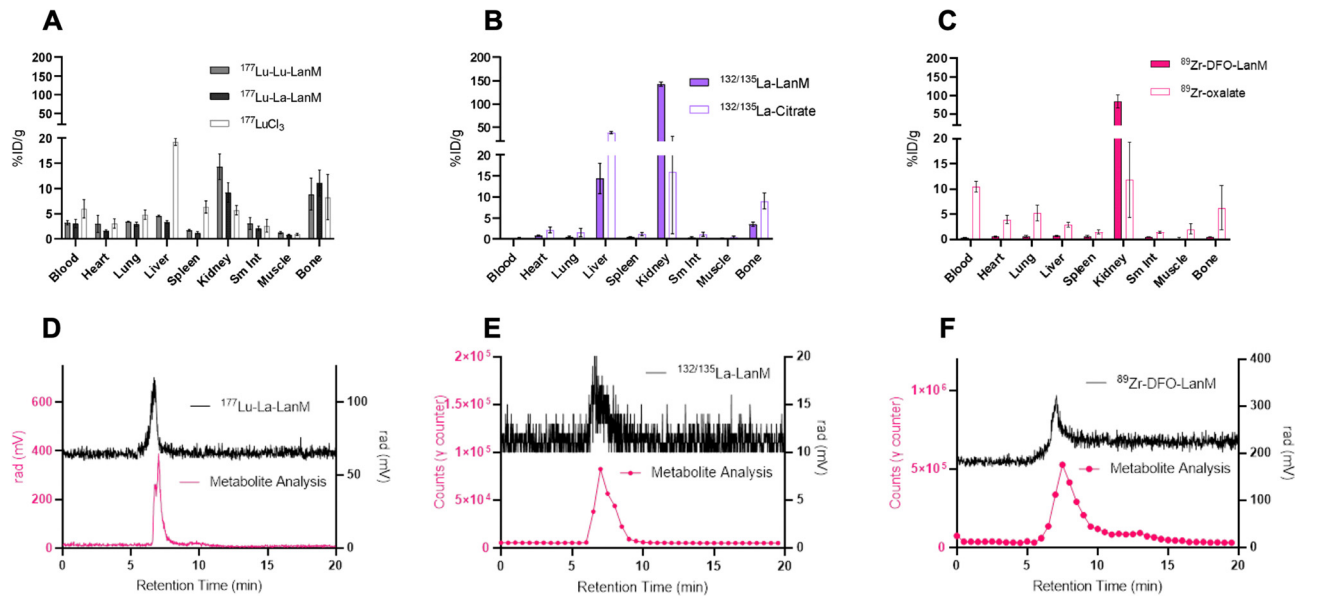

Fig. 4 (A) Two-hour post-injection biodistribution analysis of [^{177}Lu]-LanM using ^{nat}Lu (38 μCi nmol^{-1}, 68–77 μCi administered per mouse, n = 3) or ^{nat}La (35 μCi nmol^{-1}, 56–75 μCi administered per mouse, n = 4) as carrier in direct comparison with the distribution of $^{177}LuCl_3$ as the free ion surrogate (n = 3). (B) Two-hour post-injection biodistribution analysis of [$^{132/135}$La]-LanM (4 μCi nmol^{-1}, 10–14 μCi administered per mouse, n = 3) with ^{nat}La as carrier in direct comparison with the distribution of $^{132/135}$La-citrate as the free ion surrogate (n = 3). (C) Two-hour post-injection biodistribution analysis of [^{89}Zr]-DFO-LanM (40 μCi nmol^{-1}, 25–40 μCi administered per mouse, n = 5) in direct comparison with the distribution of ^{89}Zr-oxalate as the free ion surrogate (n = 3). (D) SEC-HPLC and urine metabolite analysis of [^{177}Lu]-LanM using ^{nat}La as non-radioactive carrier (E) SEC-HPLC and urine metabolite analysis of [$^{132/135}$La]-LanM. (F) SEC-HPLC and urine metabolite analysis of [^{89}Zr]-DFO-LanM.

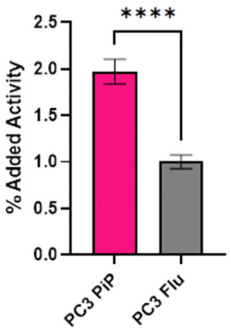

Fig. 5 Cell binding [$^{132/135}$La]-LanM-PSMA to PC3 PiP (PSMA+ cells) and PC3 Flu (PSMA− cells).

$^{132/135}$La-citrate (14.06 ± 5.13 and 17.93 ± 2.99% ID g^{-1}, respectively, Fig. S15, ESI†) was observed. The accumulation in tumor tissue remained low and differences between PSMA+ and PSMA− tumors were not statistically significant. Urine metabolite analysis confirmed residual presence of endogenously labeled [$^{132/135}$La]-LanM-PSMA (Fig. S16, ESI†). The increased deposition in bone for the LanM-PSMA conjugate relative to LanM itself may also indicate possible destabilization of protein folding with respect to the lanthanide-binding sites due to the presence of the PSMA-peptide.

Conclusions

In this study, we established protocols for the carrier-added, tracer-level radiolabeling of the lanthanide-binding protein, LanM, with medicinally relevant radioisotopes ^{177}Lu, $^{132/135}$La, and ^{89}Zr at room tempera ture using endogenous and exogenous, chemically introduced metal-binding sites. The resulting radiolabeled constructs were synthesized with 20-83% radiochemical yields and exhibited good *in vitro* stability. *In vivo* biodistribution and metabolite analysis studies revealed partial release of $^{132/135}$La and ^{177}Lu from endogenous metal binding sites, resulting in accumulation in bone and liver tissues. ^{89}Zr was efficiently retained by chelation to the exogenous DFO chelator tag, resulting in protein-mediated renal clearance.

Taken together, our data indicate that LanM constructs can be efficiently radiolabeled under desirable, mild conditions and the LanM protein exhibits pharmacokinetics comparable to other small proteins such as antibody fragments, clearing predominantly renally. Future work will focus on improving the *in vivo* stability of endogenously radiolabeled LanM to prevent dissociation of the endogenously incorporated radioisotope *in vivo*. We anticipate that overall affinity, kinetic inertness, and selectivity for Lu^{3+} relative to La^{3+} could be tuned by a combination of site-directed mutagenesis and characterization of other naturally occurring LanMs that may have distinct properties from the *M. extorquens* protein that was the subject of the present study.

Conflicts of interest

There are no conflicts to declare.

Acknowledgements

Brett Vaughn is acknowledged for help with animal experiments. K.E.M. acknowledges the SBU Chemistry-Biology interface training program (TM32GM136572). Tatiana Laremore is thanked for assistance with mass spectrometry experiments and analysis, which was performed at the Penn State Proteomics and Mass Spectrometry Core Facility, University Park, PA.

References

1 T. I. Kostelnik and C. Orvig, *Chem. Rev.*, 2019, **119**, 902–956.
2 E. W. Price and C. Orvig, *Chem. Soc. Rev.*, 2014, **43**, 260–290.
3 B. M. Zeglis and J. S. Lewis, *Dalton Trans.*, 2011, **40**, 6168–6195.
4 C. J. Anderson and M. J. Welch, *Chem. Rev.*, 1999, **99**, 2219–2234.
5 C. J. Anderson, F. Dehdashti, P. D. Cutler, S. W. Schwarz, R. Laforest, L. A. Bass, J. S. Lewis and D. W. McCarthy, *J. Nucl. Med.*, 2001, **42**, 213–221.
6 N. M. Di Bartolo, A. M. Sargeson, T. M. Donlevy and S. V. Smith, *J. Chem. Soc., Dalton Trans.*, 2001, 2303–2309, DOI: 10.1039/b103242a.
7 J. L. J. Dearling, S. D. Voss, P. Dunning, E. Snay, F. Fahey, S. V. Smith, J. S. Huston, C. F. Meares, S. T. Treves and A. B. Packard, *Nucl. Med. Biol.*, 2011, **38**, 29–38.
8 R. Rossin, P. Renart Verkerk, S. M. van den Bosch, R. C. M. Vulders, I. Verel, J. Lub and M. S. Robillard, *Angew. Chem., Int. Ed.*, 2010, **49**, 3375–3378.
9 P. Adumeau, K. E. Carnazza, C. Brand, S. D. Carlin, T. Reiner, B. J. Agnew, J. S. Lewis and B. M. Zeglis, *Theranostics*, 2016, **6**, 2267–2277.
10 J.-P. Meyer, J. L. Houghton, P. Kozlowski, D. Abdel-Atti, T. Reiner, N. V. K. Pillarsetty, W. W. Scholz, B. M. Zeglis and J. S. Lewis, *Bioconjugate Chem.*, 2016, **27**, 298–301.
11 S. M. J. van Duijnhoven, R. Rossin, S. M. van den Bosch, M. P. Wheatcroft, P. J. Hudson and M. S. Robillard, *J. Nucl. Med.*, 2015, **56**, 1422.
12 D. J. Vugts and G. A. M. S. Van Dongen, in *Radiopharmaceutical Chemistry*, ed. J. S. Lewis, A. D. Windhorst and B. M. Zeglis, Springer International Publishing, Cham, 2019, pp. 163–179, DOI: 10.1007/978-3-319-98947-1_9.
13 R. Chakravarty, S. Chakraborty, H. D. Sarma, K. V. V. Nair, A. Rajeswari and A. Dash, *J. Labelled Compd. Radiopharm.*, 2016, **59**, 354–363.
14 A. Majkowska-Pilip and A. Bilewicz, *J. Inorg. Biochem.*, 2011, **105**, 313–320.
15 A. Hu, E. Aluicio-Sarduy, V. Brown, S. N. MacMillan, K. V. Becker, T. E. Barnhart, V. Radchenko, C. F. Ramogida, J. W. Engle and J. J. Wilson, *J. Am. Chem. Soc.*, 2021, **143**, 10429–10440.
16 E. Aluicio-Sarduy, N. A. Thiele, K. E. Martin, B. A. Vaughn, J. Devaraj, A. P. Olson, T. E. Barnhart, J. J. Wilson, E. Boros and J. W. Engle, *Chem. – Eur. J.*, 2020, **26**, 1238–1242.
17 E. P. Abel, H. K. Clause, J. Fonslet, R. J. Nickles and G. W. Severin, *Phys. Rev. C*, 2018, **97**, 034312.

18 D. Emfietzoglou and H. Nikjoo, *Radiat. Res.*, 2007, **167**, 110–120.
19 J. J. Wilson, E. R. Birnbaum, E. R. Batista, R. L. Martin and K. D. John, *Inorg. Chem.*, 2014, **54**, 97–109.
20 J. A. Cotruvo Jr, E. R. Featherston, J. A. Mattocks, J. V. Ho and T. N. Laremore, *J. Am. Chem. Soc.*, 2018, **140**, 15056–15061.
21 J. A. Mattocks, J. V. Ho and J. A. Cotruvo Jr, *J. Am. Chem. Soc.*, 2019, **141**, 2857–2861.
22 G. J.-P. Deblonde, J. A. Mattocks, Z. Dong, P. T. Wooddy, J. A. Cotruvo Jr and M. Zavarin, *Sci. Adv.*, 2021, **7**, eabk0273.
23 E. R. Featherston, E. J. Issertell and J. A. Cotruvo Jr, *J. Am. Chem. Soc.*, 2021, **143**, 14287–14299.
24 Z. Dong, J. A. Mattocks, G. J.-P. Deblonde, D. Hu, Y. Jiao, J. A. Cotruvo Jr and D. M. Park, *ACS Cent. Sci.*, 2021, **7**, 1798–1808.
25 J. A. Mattocks, J. A. Cotruvo and G. J.-P. Deblonde, *Chem. Sci.*, 2022, **13**, 6054–6066.
26 G. J.-P. Deblonde, J. A. Mattocks, D. M. Park, D. W. Reed, J. A. Cotruvo Jr and Y. Jiao, *Inorg. Chem.*, 2020, **59**, 11855–11867.
27 E. C. Cook, E. R. Featherston, S. A. Showalter and J. A. Cotruvo Jr, *Biochemistry*, 2018, **58**, 120–125.
28 G. J.-P. Deblonde, J. A. Mattocks, H. Wang, E. M. Gale, A. B. Kersting, M. Zavarin and J. A. Cotruvo Jr, *J. Am. Chem. Soc.*, 2021, **143**, 15769–15783.
29 H. Singer, B. Drobot, C. Zeymer, R. Steudtner and L. J. Daumann, *Chem. Sci.*, 2021, **12**, 15581–15587.
30 E. R. Featherston, J. A. Mattocks, J. L. Tirsch and J. A. Cotruvo, in *Methods in Enzymology*, ed. J. A. Cotruvo, Academic Press, 2021, vol. 650, pp. 119–157.
31 Z. Dong, J. A. Mattocks, G. J.-P. Deblonde, D. Hu, Y. Jiao, J. A. Cotruvo and D. M. Park, *ACS Cent. Sci.*, 2021, **7**, 1798–1808.
32 S. R. Banerjee, M. Pullambhatla, C. A. Foss, S. Nimmagadda, R. Ferdani, C. J. Anderson, R. C. Mease and M. G. Pomper, *J. Med. Chem.*, 2014, **57**, 2657–2669.
33 H. M. Shallal, I. Minn, S. R. Banerjee, A. Lisok, R. C. Mease and M. G. Pomper, *Bioconjugate Chem.*, 2014, **25**, 393–405.
34 J. N. Whetter, B. A. Vaughn, A. J. Koller and E. Boros, *Angew. Chem., Int. Ed.*, 2022, **61**, e202114203.
35 B. A. Vaughn, C. S. Loveless, S. J. Cingoranelli, D. Schlyer, S. E. Lapi and E. Boros, *Mol. Pharmaceutics*, 2021, **18**, 4511–4519.
36 C. A. Umbricht, M. Benešová, R. M. Schmid, A. Türler, R. Schibli, N. P. van der Meulen and C. Müller, *EJNMMI res.*, 2017, **7**, 9.
37 D. S. Abou, T. Ku and P. M. Smith-Jones, *Nucl. Med. Biol.*, 2011, **38**, 675–681.
38 J. P. Holland, V. Divilov, N. H. Bander, P. M. Smith-Jones, S. M. Larson and J. S. Lewis, *J. Nucl. Med.*, 2010, **51**, 1293–1300.
39 S. H. Ahn, B. A. Vaughn, W. A. Solis, M. L. Lupher, T. J. Hallam and E. Boros, *Bioconjugate Chem.*, 2020, 1177–1187, DOI: **10.1021/acs.bioconjchem.0c00100**.
40 R. S. Israeli, C. T. Powell, J. G. Corr, W. R. Fair and W. D. W. Heston, *Cancer Res.*, 1994, **54**, 1807–1811.
41 D. A. Silver, I. Pellicer, W. R. Fair, W. D. W. Heston and C. Cordon-Cardo, *Clin. Cancer Res.*, 1997, **3**, 81–85.
42 C. A. Umbricht, M. Benešová, R. M. Schmid, A. Türler, R. Schibli, N. P. van der Meulen and C. Müller, *EJNMMI res.*, 2017, **7**, 9.